7-26-2007

Tuning the ferromagnetism of one-dimensional Fe / Pt / Fe multilayer barcode nanowires via the barcode layer effect

Puspamitra Panigrahi
Michigan Technological University

Ranjit Pati
Michigan Technological University

Tuning the ferromagnetism of one-dimensional Fe/Pt/Fe multilayer barcode nanowires via the barcode layer effect

Puspamitra Panigrahi and Ranjit Pati*
Department of Physics, Michigan Technological University, Houghton, Michigan 49931, USA
(Received 13 December 2006; revised manuscript received 28 February 2007; published 26 July 2007)

Using first-principles density functional theory, we have predicted equilibrium structures and electronic and magnetic properties of one-dimensional ferromagnetic Fe/Pt/Fe multilayer *barcode* nanowires. By increasing the thickness of the Pt layer and consequently reducing the thickness of the Fe layer in the nanowire in the ferromagnetic configuration, we found that the average magnetic moment per iron atom, μ_{av}, increases monotonically with an $\sim 1/N(\mathrm{Fe})$ dependence, where $N(\mathrm{Fe})$ is the number of Fe layers. The monotonic increase in average magnetic moment is attributed to the change in magnetic moment at the Fe-Pt interface, and a simple model is proposed to explain this $\sim 1/N(\mathrm{Fe})$ variation of μ_{av} in the barcode wires. Modulation of the ferromagnetism based on the number of ferromagnetic and nonmagnetic *layer sequences* in the nanowire suggests the possible application of these nanowires in nanometer scale *magnetic barcodes*. Furthermore, analysis of the Kohn-Sham energy bands in barcode nanowires suggests strong dependence of spin-polarized conductance on the nonmagnetic Pt spacer layer thickness, opening up the possibility for their application in magnetoelectronics or spintronics.

DOI: 10.1103/PhysRevB.76.024431 PACS number(s): 75.75.+a, 71.15.Mb, 73.61.At

I. INTRODUCTION

Research on magnetic and nonmagnetic heterostructures goes back to 1986, when Grünberg *et al.*[1] demonstrated for the first time the importance of interlayer exchange coupling (IEC) in Fe/Cr/Fe layered structures. Following this, the discovery of giant magnetoresistance (GMR)[2,3] in 1988 in a magnetic multilayer structure and the oscillating behavior of IEC[4] as a function of nonmagnetic layer thickness, which lead to the successful application of these materials as the read head in present day computer hard disks, intensified the interest on magnetic/nonmagnetic heterostructures. In the past few years, the nanometer scale magnetic multilayered *barcode* structure has drawn considerable attention[5–7] for its potential applications in ultrahigh sensitive magnetic sensors, high capacity magnetic storage devices, and magnetic random access memory devices.[8] Precise fabrication of barcode nanowires with the desired magnetic and nonmagnetic layer sequence is a serious challenge. In a pioneering effort, Choi *et al.*[9] have recently reported the mass fabrication of free-standing one-dimensional (1D) Co/Pt barcode nanowires with well defined layer thicknesses using programmable template-assisted deposition technique, opening up a vista for their potential applications in magnetoelectronics or spintronics.

The electronic and magnetic properties of these barcode nanowire structures are highly sensitive to the shape, thickness, and nature of the magnetic as well as nonmagnetic spacer. The presence of a nonmagnetic spacer layer of specific type and thickness between the magnetic layers in barcode structures offers additional advantages in controlling their magnetic and magnetotransport properties via tuning the IEC, an *important* theme in magnetoelectronics. Though a large number of theoretical calculations have been performed to understand the phenomenal GMR and IEC in bulk multilayers,[10–14] no first-principles theoretical calculation has been reported to understand the role of the nonmagnetic spacer in modulating the ferromagnetism of 1D multilayer barcode nanowire structures. The *challenge* associated with first-principles calculations of *isolated* 1D barcode nanowire lies in the fact that one needs to consider a large supercell with sufficient vacuum to ensure negligible interaction between the nanowire and its *image*, and to allow several spacer layers to be embedded in the nanowire structure. This increases the computational time significantly considering the spin-polarized nature of the problem. Furthermore, no *a priori* information is available on the atomic structure or stability of these nanowires compounding the theoretical task of obtaining the equilibrium barcode structures.

This work attempts to develop a fundamental understanding on the role of the nonmagnetic spacer layer in tuning the ferromagnetism of barcode nanowires. For practical purposes, we have used only two types of elements in the wire, Fe and Pt, and have concentrated only on the ferromagnetic configurations. It should be noted that the antiparallel magnetic alignment between the interlayer Fe particles on the opposite side of the Pt spacer is not considered in the present study. It would be interesting to see in the future if the antiferromagnetic coupling between the Fe particles would be more favorable over the ferromagnetic coupling. We have performed spin-polarized calculations using periodic density functional theory within local spin density approximation (LSDA).[15] The supercell structure is constructed from 39 atoms. By increasing the thickness of the Pt layer and consequently reducing the thickness of the Fe layer in the Fe/Pt/Fe barcode nanowire, we found that the average magnetic moment per Fe atom (μ_{av}) follows approximately $1/N(\mathrm{Fe})$ dependence with the number of Fe layers $N(\mathrm{Fe})$ in the nanowire. The calculated μ_{av} is 2.49 μ_B in a pristine Fe_{39} nanowire, which increases to 2.7 μ_B in $Fe_{13}Pt_{26}$, and then to 2.95 μ_B for Fe_7Pt_{32} nanowire: *barcode layer effect*. A similar barcode layer effect has recently been demonstrated experimentally in hybrid CoPt nanowires.[9] We found that the stability of the nanowire increases continuously with the in-

crease in the number of Pt layers and decrease in the number of Fe layers. A detailed analysis of the Kohn-Sham energy bands suggests a sensitive dependence of the spin-polarized conductance on the nonmagnetic Pt layer thickness.

The rest of the paper is organized as follows. A brief description of the theoretical approach is presented in Sec. II followed by the results and discussions in Sec. III. The summary of our main results are presented in Sec. IV.

II. THEORETICAL APPROACH

Determination of equilibrium structures of these magnetic nanowires from scratch is a very intricate task. We used the bulk experimental structure for fcc Fe as the guiding point for constructing the nanowire structure. Fe in the fcc phase shows a paramagnetic to ferromagnetic transition with lattice expansion. Fe nanowires constructed from bcc Fe have a smaller number of nearest neighbor atoms as compared to those constructed from fcc Fe. Besides, it has been shown recently that an ultrathin film of Fe grows in the fcc phase at the Fe-Pt interface.[16] Furthermore, the x-ray and electron diffraction studies have also reported the fcc structure for the $Fe_{50}Pt_{50}$ nanoparticle.[17] Intrigued by this, we used the fcc Fe structure and constructed a pristine Fe nanowire structure in the (111) direction which repeats itself in every three planes (*ABCABCABC*…). We placed the 39 atoms (733733733) from the periodic series (*ABCABCABC*…) in a tetragonal lattice with lattice parameter $a=18.18$ Å. The other two sides of the unit cell were taken to be 15 Å long to ensure negligible interaction between the nanowire and its image in the x and y directions. Fe/Pt/Fe barcode nanowires were constructed by layer wise replacement of Fe atoms with Pt atoms. To avoid the lattice mismatch, we choose a Pt spacer which has fcc bulk structure to construct the barcode wire. The LSDA approach, which is used for our calculation, is tested to give the correct magnetic state for fcc Fe, whereas the gradient corrected approach is found to overestimate the magnetism in fcc Fe. We have used the VASP code[18] which uses plane wave basis set and the ultrasoft pseudopotential to describe the valence-core interaction. Since geometries of these nanowires are less sensitive to the number of k points used to sample the Brillouin zone, we used $1\times1\times1$ k point mesh within the Monkhorst-Pack scheme for optimization purposes. The minimum force criterion of 0.01 eV/Å was used for each individual atom during the structural relaxation. The convergence threshold for energy was taken to be 10^{-6} eV. We used a larger $1\times1\times11$ k point (six irreducible k points) mesh for calculating the magnetic as well as electronic properties of the optimized wires. The plane wave cutoff was taken to be 237.6 eV and kept fixed for all the barcode wires studied. We used the Wigner-Seitz radii of 2.46 and 2.75 a.u. for Fe and Pt, respectively, to calculate the local magnetic moment of the individual atoms in the barcode wire. It is noteworthy to mention here that the relativistic spin-orbit interaction effect is not included in our calculation and the present calculation is based on the collinear magnetism. The noncollinear magnetic calculation is important especially for a system with multiple magnetic domains. Since the dimension of the magnetic particle in the nanowire matrix in the considered barcode wire is quite small, we have assumed the nanowire comprising single magnetic domains.

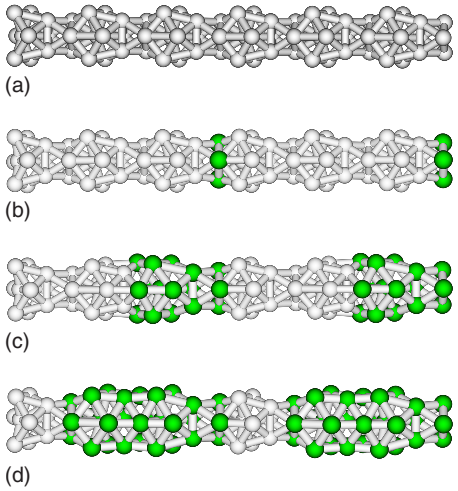

FIG. 1. (Color online) Optimized (a) Fe_{39}, (b) $Fe_{36}Pt_3$, (c) $Fe_{23}Pt_{16}$, and (d) $Fe_{10}Pt_{29}$ nanowire structures. Notation: green (dark gray), Pt; silver white (light gray), Fe.

III. RESULTS AND DISCUSSIONS

A. Structure and magnetic properties

The optimized nanowire structures are presented in Fig. 1. First, one can note a significant atomic structure relaxation in the A plane of the *ABCABCABC* unit cell in the pristine Fe nanowire. In the Fe/Pt barcode wire, the structural relaxation in the radial outward direction is noticeable (Fig. 1) in the Pt part of the wire. This is expected because the lattice parameter for bulk Pt is ~0.4 Å larger than that of fcc Fe. Next, we comment on the stability of these nanowires. To infer the stability, we calculated the cohesive energy (Fig. 2) for each wire as

$$E_C = \left(E_{NW} - \sum_i E_i\right) \Big/ N, \tag{1}$$

where E_{NW} is the energy of the nanowire, N is the number of atoms in the unit cell, and E_i corresponds to the energy of the isolated atom. One can note from Fig. 2 that the stability as well as the average magnetic moment per iron atom increase with the increase in the number of Pt spacer layers. The average magnetic moment per iron atom is calculated as

$$\mu_{av} = \frac{\sum \mu(\mathrm{Fe})}{N_{atoms}(\mathrm{Fe})}, \tag{2}$$

where $\Sigma\mu$(Fe) represents the sum of individual magnetic moments of the Fe atoms in the wire and N_{atoms}(Fe) corresponds to the total number of Fe atoms in the Fe part of the barcode wire. The pristine Fe_{39} nanowire (~0.4 nm diameter) is found to be less stable (by ~1.7 eV) than bulk fcc Fe. The average magnetic moment per atom in Fe_{39} nanowire in the ground state is found to be 2.49 μ_B compared to paramagnetic fcc bulk Fe in the ground state. Both results were obtained using similar level of theory. By increasing the di-

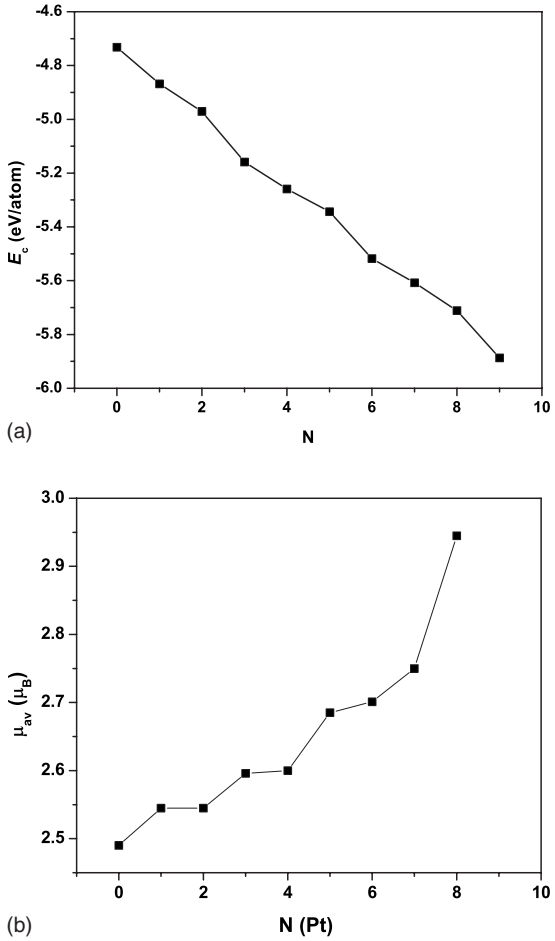

FIG. 2. Calculated (a) cohesive energy E_c and (b) magnetic moment per Fe atom μ_{av} as a function of the number of Pt layers N(Pt) in the nanowire structures.

ameter of the Fe nanowire (for ~1.1 nm diameter), we found a nearly 1 μ_B reduction in magnetic moment per atom and the stability of the ~1.1 nm diameter Fe nanowire was enhanced by ~0.9 eV relative to the ~0.4 nm diameter nanowire. Through a deeper analysis, we found that the surface Fe atom in the nanowire has higher magnetic moment of 2.7 μ_B as compared to 1 μ_B for a core Fe atom. This clearly implies that the reduced coordination number and the confinement effect along the two directions perpendicular to the length of the wire lead to the increase in magnetic moment for the 0.4 nm diameter Fe nanowire.

To understand the origin of the enhanced stability and magnetic moment per iron atom in hybrid FePt nanowire, we calculated the spin-polarized projected d-band density of states (PDOS) associated with Fe and Pt (Fig. 3). First, the discrete features in the Fig. 3 are due to a strong confinement effect. The PDOS for Fe in the pristine Fe_{39} nanowire shows strong exchange splitting with almost filled spin up d bands [Fig. 3(a)]. In the hybrid FePt structure, for example, in $Fe_{23}Pt_{16}$ nanowire, the spin up d bands are again completely filled for Fe and the 5d bands of Pt are found to be nearly degenerate with the 3d band of Fe near the Fermi energy. This suggests that there is a strong hybridization between them. The hybridization between Fe and Pt d bands leads to

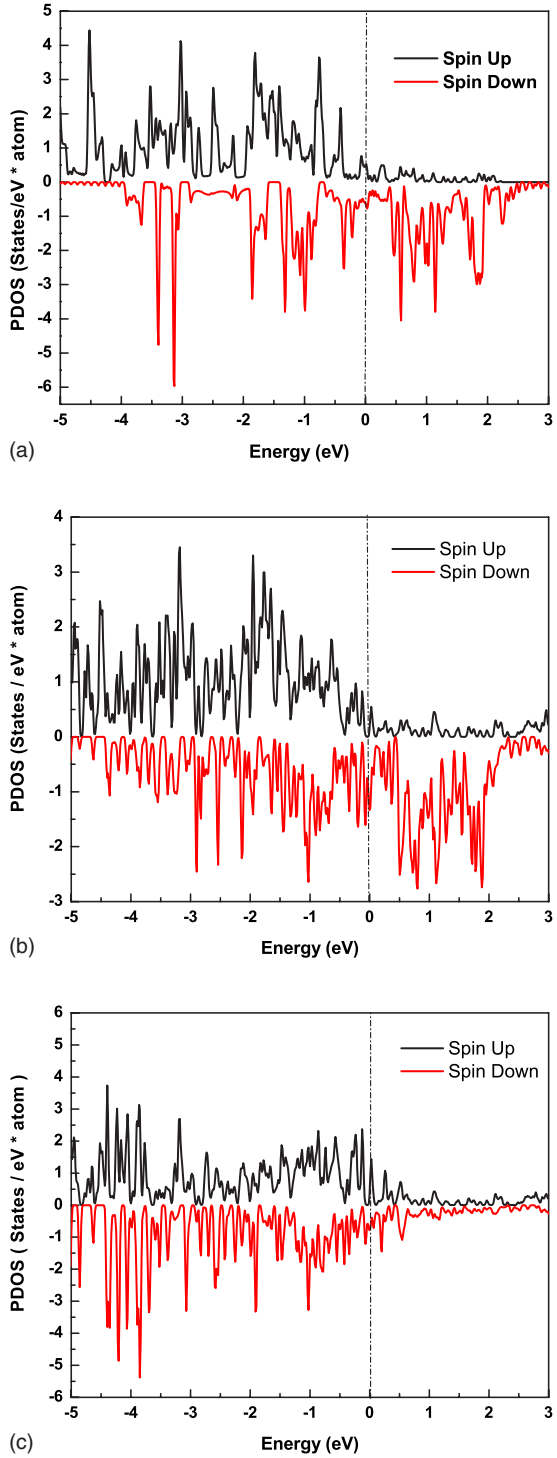

FIG. 3. (Color online) Projected spin-polarized d-band density of states (PDOS) of Fe and Pt in barcode nanowires. Spin down PDOS is plotted on the negative axis for visualization purposes: (a) Fe PDOS in Fe_{39}, (b) Fe PDOS in $Fe_{23}Pt_{16}$, and (c) Pt PDOS in the $Fe_{23}Pt_{16}$ nanowire. The Fermi level lies at E=0.

enhanced stability in the FePt system and the polarization of the Pt d band via exchange interaction. This is clearly reflected in the asymmetry between the spin up and spin down bands of Pt in Fig. 3(c). Furthermore, the hybridization between Fe and Pt at the interface weakens the hybridization

TABLE I. Comparison of individual magnetic moment (in the unit of μ_B) of Fe atoms in the pristine Fe_{39} nanowire with that of the corresponding Fe atoms in $Fe_{36}Pt_3$, $Fe_{23}Pt_{16}$, and $Fe_{10}Pt_{29}$ barcode nanowires.

Atom[a]	Fe_{39} $N(Pt)^b=0$	$Fe_{36}Pt_3$ $N(Pt)^b=1$	$Fe_{23}Pt_{16}$ $N(Pt)^b=4$	$Fe_{10}Pt_{29}$ $N(Pt)^b=7$
Fe1	1.01	1.29	1.52	1.68
Fe2	2.74	2.87	2.94	3.03
Fe3	2.74	2.80	2.79	2.85
Fe4	2.74	2.80	2.80	2.84
Fe5	2.74	2.87	2.94	3.03
Fe6	2.74	2.80	2.78	2.83
Fe7	2.74	2.87	2.94	3.03

[a]Atoms in column 1 correspond to the Fe atoms at the Fe/Pt interface in Fe-Pt barcode nanowires.
[b]N(Pt) corresponds to the number of Pt layers in the nanowire.

between the 3d bands of Fe atoms in the wire as evident from the structural analysis. We found that the nearest neighbor distance between Fe atoms in the pristine Fe_{39} nanowire is shorter (by ~0.02–0.07 Å) than that in the hybrid FePt system, especially at the Fe-Pt interface. The increased Fe–Fe bond distance leads to band narrowing and enhancement of the Fe magnetic moment in the hybrid system.

A careful inspection of the μ_{av} from Fig. 2(b) suggests that the average magnetic moment per iron atom increases monotonically with an $\sim\frac{1}{N(\mathrm{Fe})}$ dependence, where $N(\mathrm{Fe})=9-N(\mathrm{Pt})$, with $N(\mathrm{Pt})$ the number of Pt layers in the barcode nanowire. To understand this approximate $\frac{1}{N(\mathrm{Fe})}$ behavior of the μ_{av}, we analyzed the individual magnetic moments associated with the Fe and Pt atoms in the barcode nanowires. We have presented the results for individual magnetic moments for the first seven Fe atoms from the *ABCABCABC* series in Table I. For brevity, we have only presented the results for more affected interfacial atoms in the four representative nanowires in Table I. In Table I, one could see a steady monotonic increase in the magnetic moment with the decrease in N(Fe). We found that the change is more substantial for the core iron atom (Fe1) as compared to the peripheral Fe atoms. This could be understood from the interfacial structure. In the case of Fe/Pt nanowire, the core iron atom has a larger number of Pt nearest neighbors than the peripheral Fe atoms. To understand the origin of enhanced magnetic moment for the Fe atom at the Fe/Pt interface from Table I, we analyzed the up spin and down spin populations of Fe atoms both in Fe/Pt and in pristine nanowire. We found that the spin up population increases and the spin down population decreases for the Fe atoms at the Fe/Pt surface as compared to that for the corresponding Fe atoms in the pristine nanowire, suggesting spin-polarized electron transfer between the Fe and Pt layers at the interface. The larger differences in the spin up and spin down populations of the interfacial Fe atoms lead to the increased magnetic moment in the barcode nanowire.

Further examination of the individual magnetic moments suggests that the magnetic moments of the Fe, which are far away from the Fe/Pt interface, virtually remain the same as that in pristine iron nanowire. The strong electron exchange interaction between Fe and Pt at the interface induces magnetic moments on Pt layers that are closer to the interface Fe layer. The effect diminishes quickly for the Pt layers that are far from the interface. For example, in the $Fe_{10}Pt_{29}$ nanowire, we found that the Pt atoms closer to the iron layer have magnetic moment ~0.4 μ_B, whereas those Pt atoms far from the Fe layer have almost zero magnetic moment. This clearly demonstrates the role of interfacial bonding in modulating the magnetic character of the Fe atom.

B. Model for magnetic moment variation

Since the introduction of Fe/Pt interface increases the local magnetic moment of the interfacial Fe atoms compared to that in pristine Fe nanowire, one could write the average magnetic moment per iron atom in Fe/Pt hybrid nanowire as

$$\mu_{av}=\mu_{av}(\mathrm{pristine})+d\mu_{av}, \tag{3}$$

where μ_{av}(pristine) is the average magnetic moment per iron atom in pristine Fe_{39} nanowire. The $d\mu_{av}$ is the average contribution from the interface structure and can be approximated as

$$d\mu_{av}\propto\frac{N_{\text{Fe-Pt}}}{N_{\text{Fe atoms}}}, \tag{4}$$

where $N_{\text{Fe-Pt}}$ is the number of nearest neighbor Fe atoms of the Pt interface and $N_{\text{Fe atoms}}$ is the total number of Fe atoms in the barcode wire. Since μ_{av}(pristine) is constant for all the barcode wires, the variation observed comes from the interface structure. For example, in barcode wires with $N(\mathrm{Fe})=1, 2, 3, 4, 5, 6, 7, 8$, one can find $N_{\text{Fe-Pt}}=14, 10, 10, 14, 10, 10, 14, 10$ and $N_{\text{Fe atoms}}=7, 10, 13, 20, 23, 26, 33, 36$. In our 39-atom (*ABCABCABC*) unit cell, for $N(\mathrm{Fe})=1$, we have one interface between *A* iron layer (seven atoms) and *B* platinum layer (three atoms), and another interface between the end *C* platinum layer (three atoms) and the *A* iron layer (seven atoms) of the next unit cell, resulting to $N_{\text{Fe-Pt}=}14$. A similar approach is used to obtain all the elements of the $N_{\text{Fe-Pt}}$ series. Calculating the μ_{av} from the simple model in Eqs. (3) and (4) and plotting them as a function of N(Pt), we find a similar trend as shown in Fig. 2(b). The small discrepancy of the trend in Fig. 2(b) is attributed to the exact nature of the interfacial electronic structure, which is absent in the simple model [Eqs. (3) and (4)]. Crudely, this variation in μ_{av} follows approximately a $\frac{1}{N(\mathrm{Fe})}$ trend with N(Fe). The small oscillatory change from $\frac{1}{N(\mathrm{Fe})}$ could be understood from the nonuniform increase in the number of iron atoms with N(Fe). Though this simple model presented in Eqs. (3) and (4) could explain the monotonic increase in magnetic moment of the iron with the decrease in N(Fe), it remains to be seen whether it can explain other 1D barcode structures.

C. Spin-polarized energy bands

To get deeper insights into the electronic properties, we have calculated the spin-polarized Kohn-Sham energy bands

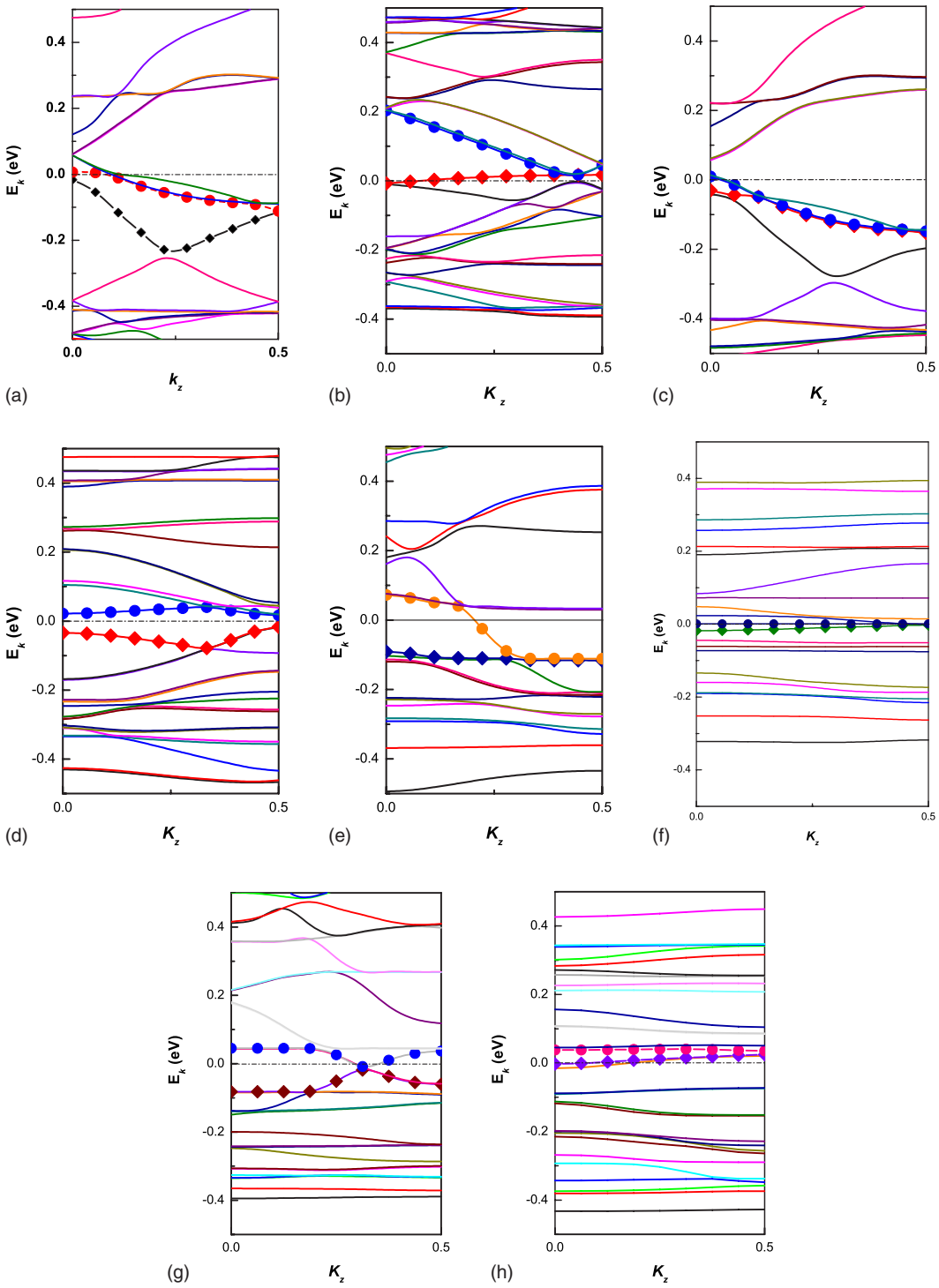

FIG. 4. (Color online) Spin-polarized electronic band structures for (a) Fe_{39} (spin up), (b) Fe_{39} (spin down), (c) $Fe_{36}Pt_3$ (spin up), (d) $Fe_{36}Pt_3$ (spin down), (e) $Fe_{23}Pt_{16}$ (spin up), (f) $Fe_{23}Pt_{16}$ (spin down), (g) $Fe_{10}Pt_{29}$ (spin up), and (h) $Fe_{10}Pt_{29}$ (spin down) nanowires. The Fermi level lies at $E=0$. The band with solid circles corresponds to the conduction band, and the band with solid diamonds corresponds to the valence band.

of these nanowires (Fig. 4). A strong exchange splitting in the band structures is clearly evident in the pristine Fe_{39} nanowire. In the spin up case, the conduction band crosses the Fermi energy. In contrast, the valence band in the spin down case crosses the Fermi energy. This suggests that both the spin up and down channels could contribute to the total conductance of $G_0 \approx 2e^2/h$ in this wire assuming an ideal transmission ($T \approx 1$) for each spin channel and ignoring spin flip scattering. In the case of the $Fe_{36}Pt_3$ nanowire, there is a gap opening in the spin down case and only the spin up conduction band crosses the Fermi energy. One would thus expect only the majority spin band to contribute to the con-

ductance ($\sim 0.5\ G_0$) near the Fermi energy. For the $Fe_{23}Pt_{16}$ wire, we found a gap closure in the spin down channel and the spin up conduction band again crosses the Fermi energy, suggesting that both spin up and spin down channels would contribute to the conduction as in the pristine Fe_{39} nanowire. In the case of the $Fe_{10}Pt_{29}$ nanowire, one can notice a small gap opening between the spin down conduction and valence bands as compared to that in $Fe_{23}Pt_{16}$ nanowire. These results, in fact, suggest that the spin-polarized conductance in these barcode wires can be controlled by controlling the number of Pt spacer layers. The dependence of spin-polarized conductance on the number of Pt layers in the barcode wire offers interesting possibilities in controlling magnetoconductance properties of these wires via precise control of the number of ferromagnetic and nonmagnetic layer sequences in the wire, opening up the possibility for their application in magnetoelectronics. Another most intriguing feature we found in the band structure is the occurrence of dispersionless flatbands in the hybrid FePt nanowire. We found that the occurrences of flatbands near the Fermi energy are more prominent in the $Fe_{23}Pt_{16}$ and $Fe_{10}Pt_{29}$ nanowire. To understand this unique feature in the energy bands, we recalculated the Kohn-Sham energy bands of the $Fe_{10}Pt_{29}$ nanowire by removing all the Pt layers from the wire. The almost negligible orbital overlap between the Fe_{10} nanoclusters in the nanowire leads to dispersionless flatbands. This further confirms the localize nature of magnetic moment modification of the Fe atom at the Fe/Pt interface. Thus, it is safe to assign these flatbands we observe in Figs. 4(e)–4(h) near the Fermi energy to the $3d$ bands of the Fe atoms in the wire.

IV. CONCLUSIONS

In summary, the results presented in this paper clearly illustrate the role of nonmagnetic spacer layer thickness in modulating the magnetic and electronic properties of multilayer barcode nanowire. Particularly, our first-principles calculations suggest that by increasing the thickness of the Pt layer and consequently reducing the thickness of the Fe layer in the Fe/Pt/Fe barcode nanowire, the average magnetic moment per Fe atom increases monotonically from 2.49 μ_B in the pristine Fe_{39} nanowire to 2.7 μ_B in the $Fe_{13}Pt_{26}$ nanowire and then to 2.95 μ_B in the Fe_7Pt_{32} nanowire. This is the *barcode layer effect*. The monotonic increase in average magnetic moment is attributed to the change in magnetic moment at the Fe-Pt interface, and we have proposed a simple model based on this interface structure to explain the $\sim\frac{1}{N(\mathrm{Fe})}$ trend in μ_{av} obtained from first-principles density functional calculations. Tuning ferromagnetism via precise control of ferromagnetic and nonmagnetic layer sequences in barcode nanowire, which has been demonstrated experimentally by Choi *et al.*[9] in the CoPt system, is expected to open up the possibility for their application in nanoscale *magnetic barcodes*. The strong dependence of spin-polarized energy bands in the vicinity of the Fermi energy on the nonmagnetic layer thickness further suggests the potential applications of these nanoscale barcode structure in magnetoelectronics or spintronics.

ACKNOWLEDGMENTS

We thank N. W. Ashcroft, A. C. Pineda, and M. Cinal for helpful discussions during this work. This work was partially supported by National Computational Science Alliance under Grants No. ASC060031T and TG-ASC070026N.

*patir@mtu.edu

[1] P. Grünberg, R. Schreiber, Y. Pang, M. B. Brodsky, and H. Sowers, Phys. Rev. Lett. **57**, 2442 (1986).
[2] M. N. Baibich, J. M. Broto, A. Fert, Nguyen Van Dau, F. Petroff, P. Etienne, G. Creuzet, A. Friederich, and J. Chazelas, Phys. Rev. Lett. **61**, 2472 (1988).
[3] G. Binasch, P. Grünberg, F. Saurenbach, and W. Zinn, Phys. Rev. B **39**, 4828 (1988).
[4] S. S. P. Parkin, N. More, and K. P. Roche, Phys. Rev. Lett. **64**, 2304 (1990).
[5] A. Blondel, J. P. Meier, B. Doudin, and J.-Ph. Ansermet, Appl. Phys. Lett. **65**, 3019 (1994).
[6] L. Piraux, J. M. George, J. F. Despres, C. Leroy, E. Ferain, R. Legras, K. Ounadjela, and A. Fert, Appl. Phys. Lett. **65**, 2484 (1994).
[7] M. Tanase, D. M. Silevitch, A. Hultgren, L. A. Bauer, P. C. Searson, G. J. Meyer, and D. H. Reich, J. Appl. Phys. **91**, 8549 (2002).
[8] G. A. Prinz, Science **282**, 1660 (1998).
[9] J. Choi, S. J. Oh, H. Ju, and J. Cheon, Nano Lett. **5**, 2179 (2005).
[10] P. Bruno, Phys. Rev. B **52**, 411 (1995).
[11] D. Stoeffler and F. Gautier, Phys. Rev. B **44**, 10389 (1991).
[12] P. Lang, L. Nordström, R. Zeller, and P. H. Dederichs, Phys. Rev. Lett. **71**, 1927 (1993).
[13] M. van Schilfgaarde and F. Herman, Phys. Rev. Lett. **71**, 1923 (1993).
[14] B. Skubic, E. Holmström, D. Iusan, O. Bengone, O. Eriksson, R. Brucas, B. Hjörvarsson, V. Stanciu, and P. Nordblad, Phys. Rev. Lett. **96**, 057205 (2006).
[15] R. G. Parr and W. Yang, *Density-Functional Theory of Atoms and Molecules* (Oxford Science, New York, 1994).
[16] D. Repetto, T. Y. Lee, S. Rusponi, J. Honolka, K. Kuhnke, V. Sessi, U. Starke, H. Brune, P. Gambardella, C. Carbone, A. Enders, and K. Kern, Phys. Rev. B **74**, 054408 (2006).
[17] B. Stahl, N. S. Gajbhiye, G. Wilde, D. Kramer, J. Ellrich, M. Ghafari, H. Hahn, H. Gleiter, J. Weibmuller, R. Wurschum, and P. Schlossmacher, Adv. Mater. (Weinheim, Ger.) **14**, 24 (2002).
[18] Vienna ab initio simulation package, Technische Universität Wien, 1999; G. Kresse and J. Furthmüller, Phys. Rev. B **54**, 11169 (1996).